Deciphering the Mechanism of Crystallization of UiO-66 Metal-Organic Framework

Olesya O. Semivrazhskaya, Daniil Salionov, Adam H. Clark, Nicola P. M. Casati, Maarten Nachtegaal, Marco Ranocchiari, Saša Bjelić, René Verel, Jeroen A. van Bokhoven, and Vitaly L. Sushkevich*

Zirconium-containing metal-organic framework (MOF) with UiO-66 topology is an extremely versatile material, which finds applications beyond gas separation and catalysis. However, after more than 10 years after the first reports introducing this MOF, understanding of the molecular-level mechanism of its nucleation and growth is still lacking. By means of in situ time-resolved high-resolution mass spectrometry, Zr K-edge X-ray absorption spectroscopy, magic-angle spinning nuclear magnetic resonance spectroscopy, and X-ray diffraction it is showed that the nucleation of UiO-66 occurs via a solution-mediated hydrolysis of zirconium chloroterephthalates, whose formation appears to be autocatalytic. Zirconium-oxo nodes form directly and rapidly during the synthesis, the formation of pre-formed clusters and stable non-stoichiometric intermediates are not observed. The nuclei of UiO-66 possess identical to the crystals local environment, however, they lack long-range order, which is gained during the crystallization. Crystal growth is the rate-determining step, while fast nucleation controls the formation of the small crystals of UiO-66 with a narrow size distribution of about 200 nanometers.

1. Introduction

Metal-organic frameworks (MOFs) have been studied in depth by chemists and material scientists because of their tunable porosity and diversity of discovered topologies.[1,2] Importantly, they are not rigid structures and can undergo post-synthetic modification, enabling adjustment and fine-tuning of their chemical and physical properties.[3–12] Due to these unique features, MOFs are studied and applied in many fields, from gas adsorption and separation, to energy storage and (electro) catalysis.[1–12]

Not every MOF attracts the same degree of attention from researchers, interest depends on the intrinsic properties of each particular metal-organic framework, high porosity, (solvo)thermal stability and mechanical durability are at the forefront.[1,2,6,12] One of these most

O. O. Semivrazhskaya
Laboratory for Organic Chemistry
ETH Zurich
Vladimir-Prelog-Weg 3, 8093 Zurich, Switzerland
D. Salionov, S. Bjelić
Bioenergy and Catalysis Laboratory
Paul Scherrer Institute
5232 Villigen PSI, Switzerland
A. H. Clark, M. Nachtegaal
Operando Spectroscopy Group
Paul Scherrer Institute
5232 Villigen PSI, Switzerland

N. P. M. Casati
Laboratory for Synchrotron Radiation—Condensed Matter
Paul Scherrer Institute
5232 Villigen PSI, Switzerland
M. Ranocchiari, J. A. van Bokhoven, V. L. Sushkevich
Laboratory for Catalysis and Sustainable Chemistry
Paul Scherrer Institute
5232 Villigen PSI, Switzerland
E-mail: vitaly.sushkevich@psi.ch
R. Verel, J. A. van Bokhoven
Institute for Chemistry and Bioengineering
ETH Zurich
Vladimir-Prelog-Weg 1, 8093 Zurich, Switzerland

**ADVANCED
SCIENCE NEWS**

www.advancedsciencenews.com

NANO · MICRO

small

www.small-journal.com

promising and fascinating MOFs is UiO-66, comprising $[Zr_6(OH)_4O_4]^{12+}$ oxo-clusters and terephthalate linkers, which form cubic cells.[13,14] The steadily increasing number of publications devoted to UiO-66 has paved the way for current research into structure-performance relationships, (that are approaching maturity) which reveal new challenges to be met.[15] One of these is understanding the synthesis of UiO-66 at the molecular level, which is essential to achieve further progress in reproducible synthesis and modulating the size and shape of the crystals, targeted for scale-up and standardization.[16,17] Studying the formation of metal-organic frameworks is complex due to the heterogeneity of the synthesis medium, which comprises a solvent, an inorganic precursor, an organic linker, a modulator, and a deprotonating agent, as well as the high sensitivity to physical and chemical parameters, such as temperature, pH, concentration, and aging time.[18–21] These issues are highlighted in recent reviews[22–26] as well as in our recent publication,[27] urging researchers to develop and use in situ methods for monitoring synthesis.

A number of research papers focus on the in situ analysis of the formation of UiO-66 under solvothermal conditions, mostly by means of X-ray scattering techniques, which are intrinsically sensitive to crystalline phases and, in some cases, to the amorphous nuclei.[21,28–30] In this way, the effect of the modulator, such as minerals and organic acids, on the crystallization kinetics can be studied and linked to the crystal size distribution of the final product. Further fitting of the crystallization curve, based on Gualtieri,[31] Avrami-Erofeev[32] or Sharp-Hancock[33] models, enables the extraction of nucleation and growth parameters. The researchers reached the conclusion that the addition of modulators, deprotonating agents, and water to the synthetic mixture accelerates the synthesis, which results in UiO-66 crystals of different sizes. However, the molecular mechanism of such control cannot be derived from wide- and small-angle X-ray scattering alone.

Using methods not requiring long-range ordering, such as X-ray total scattering and pair distribution function (PDF) analysis, an elementary mechanism, involving growth from pre-formed clusters, was suggested for amino-functionalized UiO-66.[34,35] However, PDF data are not element-specific and are complex, they do not provide information about the chemical processes that take place during the synthesis. From this perspective, NMR spectroscopy is a powerful tool to follow these chemical transformations. For instance, ^{1}H NMR showed the evolution of water and solvent signals during the synthesis, for the most part showing the formation of various adducts and their temporal behavior, with no clear relationship to the evolution of the terephthalate linker in the context of nucleation and/or the crystallization process.[36]

There is not one single technique that can interrogate the evolution of all species during MOF synthesis and follow their evolution on timescales from seconds to days. In our previous work,[27] we showed that the MIL-53 crystallization mechanism can now be studied in great depth by combining in situ electrospray ionization coupled to high-resolution mass spectrometry (ESI-HRMS), magic angle spinning NMR (MAS NMR) and X-ray diffraction (XRD).

In the present work, we employed the developed methodology to monitor the formation of UiO-66, starting from the induc-

tion period through nucleation to the crystal growth. Our toolkit was reinforced by time-resolved Zr K-edge X-ray absorption spectroscopy (XAS), employing Fourier and wavelet analysis (WT) of EXAFS. The application of several spectroscopic techniques enabled us to follow the fate of zirconium atoms as well as that of the terephthalic linker, water, and *N, N*-dimethylformamide (DMF) as solvent. These data were complemented by those of X-ray diffraction and revealed the molecular mechanism of UiO-66 crystallization. Zirconium chloroterephthalates play a key role in the initiation of nucleation, which proceeds via a solution-mediated mechanism. The pre-formation of $[Zr_6(OH)_4O_4]^{12+}$ clusters via hydrolysis of $ZrCl_4$ does not take place, instead, these clusters formed rapidly during the irreversible hydrolysis of soluble zirconium chloroterephthalates. DMF undergoes hydrolysis, catalyzed by HCl, leading to dimethylammonium chloride and formate species, which are preserved in the solution. The complexity of UiO-66 crystallization chemistry justifies the need for a case-by-case MOF synthesis investigation across the time domain.

2. Results

2.1. High-Resolution Mass Spectrometry

HRMS spectrometry was used to analyze the composition of the synthetic mixture at short reaction time. Right after the dissolution of zirconium chloride and terephthalic acid (H_2BDC) in a mixture of *N, N*-dimethylformamide and hydrochloric acid, various compounds are formed. **Figure 1**A,B reports exemplary ESI-HRMS spectra, recorded in negative and positive modes, respectively. Even though zirconium chloride that was used in the mass spectrometry experiments was labeled with a single ^{90}Zr isotope, the natural isotopic distribution of chlorine, represented by the ^{35}Cl / ^{37}Cl mixture, leads to the appearance of multiple peaks in the spectrum of individual adducts. The unambiguous assignment of the signals required further isotope labeling, which in turn enabled the detection of the most intense peaks in the range of 100–1000 *m/z* (Figures S1 and S2, Tables S1 and S2, Supporting Information). As well as the $ZrCl_5^-$ anion, resulting from the dissociation of the initial zirconium chloride, a family of different zirconium chloroterephthalates with the formula $[ZrCl_{5-x}(HBDC)_x]^-$, $1 < x < 5$ was found (**Scheme 1**). These are formed by the gradual substitution of chlorine in zirconium chloride by terephthalate. A smaller fraction of zirconium chloroterephthalates, containing two Zr atoms, was also detected. Due to the dilution of the samples with methanol prior to the injection into the mass spectrometer, methoxy species may participate in the exchange, as seen clearly in the corresponding spectra, in which $ZrCl_3(HBDC)(OCH_3)^-$ and $ZrCl_2(HBDC)_2(OCH_3)^-$ are visible. Finally, the signals of copper and iron chlorides originate from the impurities that are always present in hydrochloric acid.[37] Extraction of quantitative information from ESI-MS was not possible due to the significantly varied intensity of the signals.

The spectrum acquired in positive mode is dominated by the signals resulting from the dimethylformamide hydrolysis products, in particular, dimethylammonium chlorides with the formula $[((CH_3)_2NH_2)_{x+1}Cl_x]^+$, $1 < x < 10$. Moreover, the dimethylammonium cation in these adducts undergoes exchange with

ADVANCED
SCIENCE NEWS
www.advancedsciencenews.com

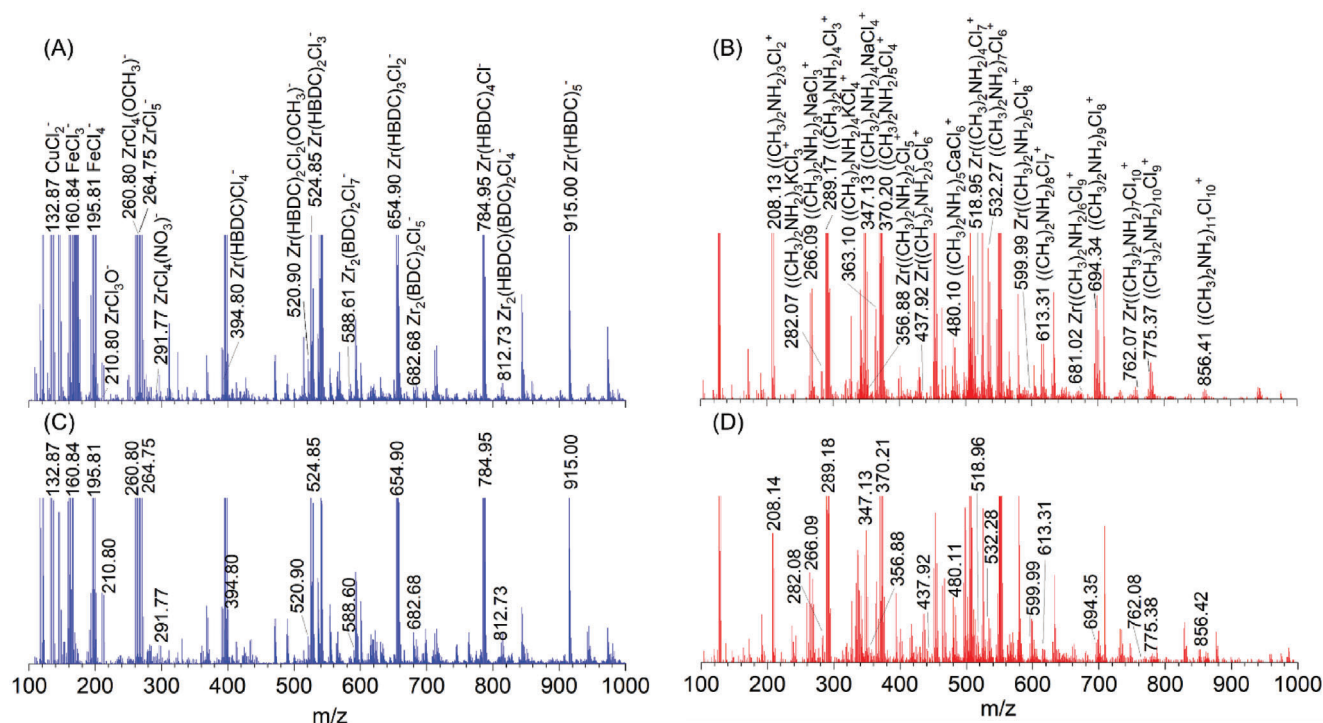NANO · MICRO
small
www.small-journal.com

Figure 1. ESI Q-TOF mass spectra of the synthetic mixture after 30 min measured in A) negative and B) positive modes, respectively. The same spectra were collected during the reaction with $H_2{}^{18}O$-labeled water, (C) and (D), respectively. The reaction was carried out at 363 K, and the samples were diluted with methanol (1:100 v/v) prior to injection into to mass spectrometer. The most intense peaks belong to the different families of zirconium chloroterephthalates and dimethylammonium chlorides. The methoxy group in some of the peaks originates from methanol, the HRMS solvent. The *m/z* values are provided for monoisotope compounds comprising ^{90}Zr and ^{35}Cl isotopologues. Tables S1 and S2, Supporting Information, give the complete description of the spectra together with the peak assignment.

zirconium atoms and forms $[Zr((CH_3)_2NH_2)_xCl_{x+3}]^+$ or other alkali or alkali-earth metals (Table S2, Supporting Information). At a reaction time longer than 2 h, dimethylammonium chloride salts represent the main products left in the solution at the end of UiO-66 crystallization (Figure S3, Supporting Information). In contrast to MIL-53, no DMF-containing adducts were found, which explains the weak interaction of Zr cations with dimethylformamide,[27] in line with the hard-soft acid-base principle.

Unexpectedly, we did not find any Zr-oxo adducts in the solution, which might be indicative of the partial hydrolysis of $ZrCl_4$ with the formation of precursors of secondary building units (SBUs).[34,35] This was supported by the experiment with oxygen-18 labeled water, which was used instead of unlabeled hydrochloric acid. A priori, in the case of the formation of zirconium (hydr)oxo species, there should be a shift M+2 in the corresponding spectra compared to the data set produced with an unlabeled aqueous synthetic mixture. However, this is not the case
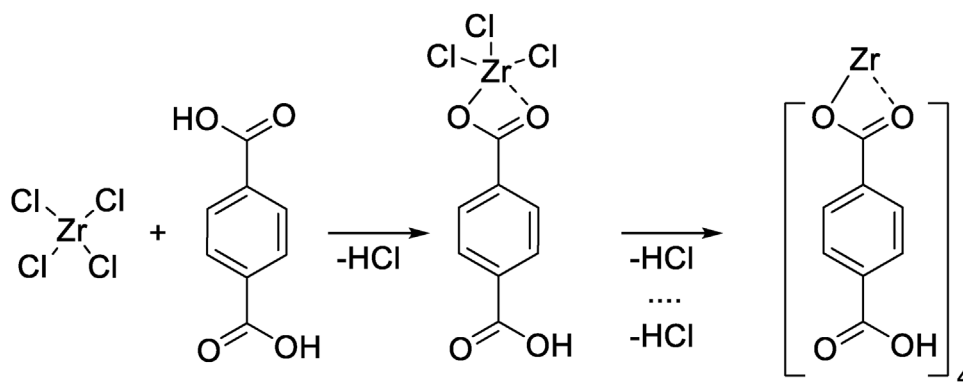
Scheme 1. Exchange reaction between zirconium chloride and terephthalic acid leading to zirconium chloroterephthalates with different degree on substitution.

**ADVANCED
SCIENCE NEWS**

www.advancedsciencenews.com

**NANO · MICRO
small**

www.small-journal.com

(Figure 1C,D): Utilization of $H_2^{18}O$ does not lead to a change in the position of the HRMS peaks, including those, which were not assigned, indicating the absence of volatile zirconium (hydr)oxo species. We tentatively suggest that this might be related to the formation of insoluble SBUs, which rapidly convert into the UiO-66 nuclei (vide infra).

2.2. In Situ Zr K-Edge X-Ray Absorption Spectroscopy

Being element-specific and sensitive to the local bonding environment only (≈ 5 Å), X-ray absorption spectroscopy is ideally suited to observe zirconium atoms during the synthesis, providing quantitative information about the redistribution of Zr among the crystalline, amorphous, and liquid phases. **Figure 2**A displays exemplary time-resolved Zr K-edge XANES spectra acquired during the crystallization of UiO-66 at 373 K. The shape and intensity of the white line undergo significant changes: The spectrum of the initial mixture resembles that of bulk zirconium chloride with three resolved peaks at 18 015, 18 023, and 18 032 eV, while the final state spectrum is identical to that of UiO-66 synthesized ex situ, giving a single intense signal at 18 021 eV (Figure S4, Supporting Information). No traces of zirconium oxide were detected (Figure S4, Supporting Information). Figure 2B shows k3-weighted FT EXAFS spectra, showing the evolution of the Zr local environment during the synthesis. The initial spectrum consists of a single coordination shell, belonging to the Zr–Cl scattering, the intensity of which decreases progressively during the reaction. After the induction period, a peak corresponding to the second coordination sphere appears at about 3.1 Å (phase non-corrected) and develops gradually. The assignment of this peak to Zr–Zr scattering in the $[Zr_6(OH)_4O_4]$ node is confirmed by the wavelet analysis, the results of which are presented in Figure 2C.[14] The emerging lobe, centered at (9.0 Å^{-1}, 3.1 Å) in the WT contour plot, is due to the scattering of the zirconium atoms with a high Z number. Apart from that, WT EXAFS indicates the increasing contribution of oxygen scattering to the first coordination sphere, as revealed by the gradual shift of the center of the corresponding lobe from (6.2 Å^{-1}, 2.0 Å) to (5.0 Å^{-1}, 1.7 Å). This is in line with the FT EXAFS data, which show a double peak in the first coordination sphere due to different oxygen atoms at two distinct bond distances in the UiO-66 structure. Finally, Figure 2B shows the presence of an additional weak peak at about 4.6 Å in the phase-uncorrected EXAFS spectra, which originates from other Zr atoms in the $[Zr_6(OH)_4O_4]$ node.[14] A comparison of the integral intensity of the FT EXAFS peaks of the Zr–Zr scatterings at d(Zr–Zr$_1$) = 3.1 Å and d(Zr–Zr$_2$) = 4.6 Å[13,14] shows that both Zr neighbors appear and develop simultaneously (Figure S5, Supporting Information).

Further analysis of the time-resolved XAS series collected at different reaction temperatures, was performed by means of principal component analysis. At least three linearly independent components are required to describe the entire array of data. Utilization of two components does not allow for a reliable fit of the initial period of the reaction, while the 4-component fit overfits the data sets (please see Figures S6 and S7, Supporting Information and discussion in Supporting Information). **Figure 3**A–D shows Zr K-edge XANES, k^3-weighted FT EXAFS, k^3-weighted WT EXAFS, and the temporal behavior of the resolved princi-

pal components (denoted PC1, PC2, and PC3) (Figure S8, Supporting Information). The XANES spectrum of PC1 resembles that of ZrCl$_4$ dissolved in DMF, the fitting of the k^3-weighted FT EXAFS spectrum results in a Zr–Cl distance of 2.45 ± 0.01 Å with a corresponding coordination number of 8 ± 0.4 (Figure S9 and Table S3, Supporting Information). The concentration profile (Figure 3D) indicates rapid, complete, and irreversible transformation of the species associated with PC1. Unexpectedly, the decrease in the fraction of the PC1 component follows an accelerating shape of the curve, which is typical of autocatalytic reactions.[30,38] Importantly, an increase in the reaction temperature increases the rate of the reaction, this does not, however, change the accelerating nature of the autocatalytic process within the range of 353–373 K.

The XANES spectrum of the PC2 component shows a slight variation with respect to that of PC1, which indicates the presence of a substantial number of chlorine atoms surrounding zirconium. This assumption was confirmed by fitting the weighted FT EXAFS spectrum, which derives a Zr-Cl distance of 2.47 ± 0.01 Å with a decrease in the coordination number to 7 ± 0.4 (Figure S10 and Table S3, Supporting Information). This is rationalized in terms of the formation of zirconium chloroterephthalates, in line with the HRMS data. Notably, the EXAFS spectrum of PC2 does not contain any pronounced peaks in the second and third coordination shells. The concentration profiles are typical of reaction intermediates, possessing clear maxima whose positions depend on the reaction temperature, hence shifting to shorter reaction times with increasing temperature. Moreover, the position of the maxima coincides with the attainment of the full conversion of the PC1-associated species.

When the maximum PC2 concentration is reached, the fraction of PC3 starts to increase gradually (Figure 3D). The shape of the concentration profile is characteristic of a nucleation/crystallization curve, which starts with an induction period and then follows a sigmoid-like shape.[31–33] The resolved XANES spectrum is significantly different from that of PC1 and PC2 and is identical to that of the crystalline UiO-66 phase. The fitting of the EXAFS spectrum confirms the assignment of PC3 to zirconium in UiO-66 (Figure S11 and Table S3, Supporting Information).[14] Hence, the XAS data confirm that the formation of UiO-66 proceeds via the zirconium chloroterephthalate intermediates, which are formed via an autocatalytic reaction. Hydrolysis of the latter leads to the direct formation of UiO-66 species with no observable hydro(oxo) intermediates, in line with the HRMS data.

2.3. In Situ MAS NMR Spectroscopy

While XAS enables the determination of the structure of the Zr atoms in the molecular precursor and the secondary-building units of UiO-66, MAS NMR follows the fate of the terephthalate linker and monitors the evolution of water and HCl signals. Direct excitation probes, for the most part, the liquid phase and the soluble species, whereas CP-MAS spectroscopy is intrinsically sensitive to the rigid species, such as nuclei and crystallites.[27,39] **Figure 4** represents exemplary time-resolved ^{13}C without proton decoupling, NODEC, (A), ^1H-^{13}C CP-MAS (B), and ^1H (C) NMR spectra, acquired during the synthesis of UiO-66 at 353 K.

ADVANCED
SCIENCE NEWS

www.advancedsciencenews.com
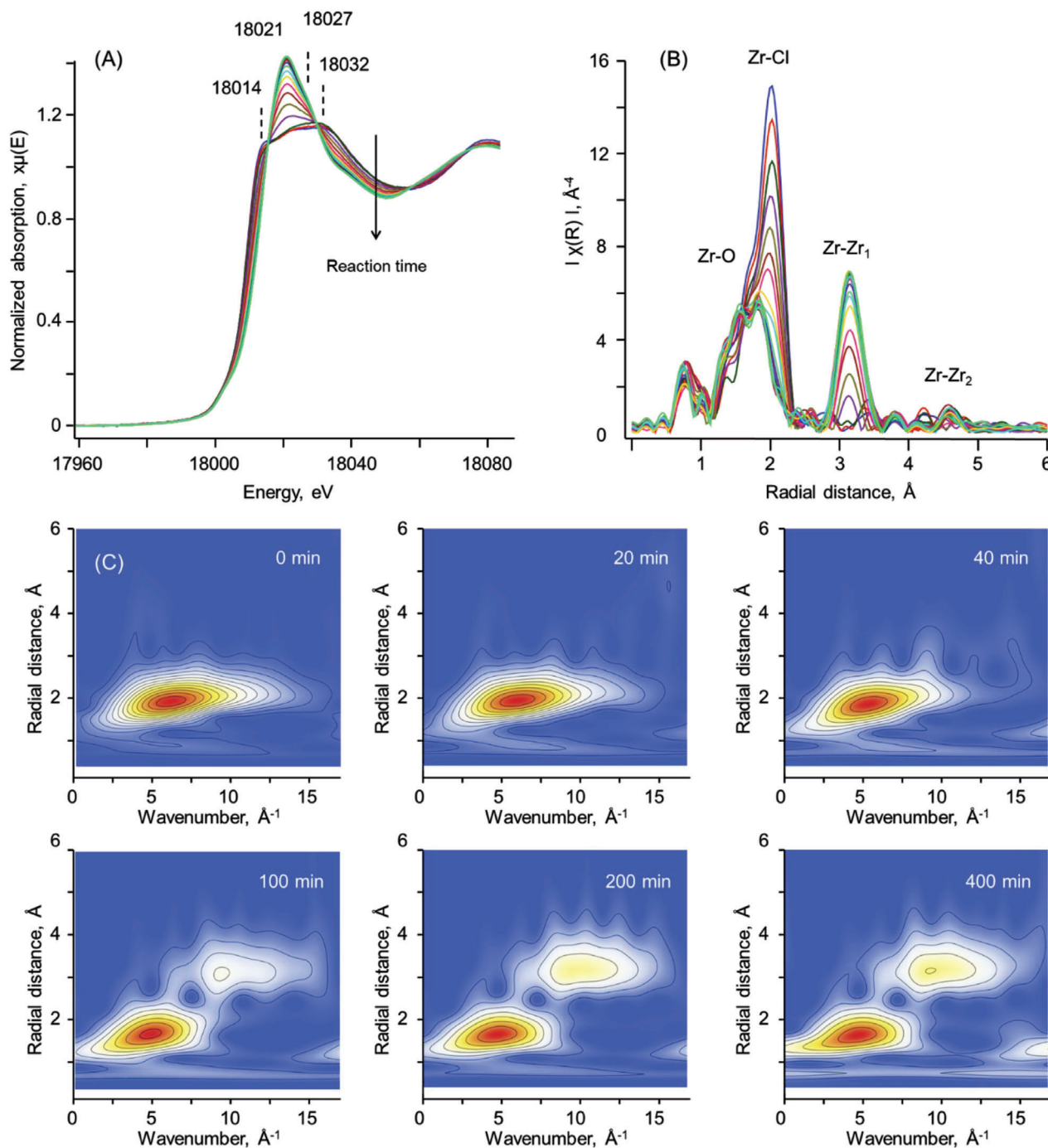
NANO · MICRO

small

www.small-journal.com

Figure 2. A) Exemplary time-resolved Zr K-edge XANES spectra. Upon reaction there is a clear change in the white line shape together with the edge shift to higher energy. B) Exemplary time-resolved Zr K-edge k^3-weighted FT EXAFS spectra. Zr-O and Zr-Cl contributions are clearly visible in the first coordination shell, with Zr–Zr scattering contributing to the second shell, respectively. C) Exemplary time-resolved Zr K-edge k^3-weighted WT EXAFS spectra. Initial mixture characterized by the presence of the single lobe due to Zr–Cl and Zr–O scatterings, while at longer reaction time, a lobe due to Zr–Zr appears and gradually develops. The reaction temperature was 373 K.

The signal at about 167 ppm in the ^{13}C NMR spectra corresponds to the terephthalate species located in the synthetic solution, while the triplet at 163 ppm is due to the solvent, deuterated dimethylformamide. During the reaction, the intensity of the terephthalate signal decreases and reaches ≈0.05 M concentration, which is associated with the stoichiometric excess of terephthalic acid used for the synthesis. The concentration profile of terephthalate (Figure 4D), derived from the integration of the NMR signal, reveals a notable behavior: The reaction starts from the plateau at about 0.15 M, followed by the exponential
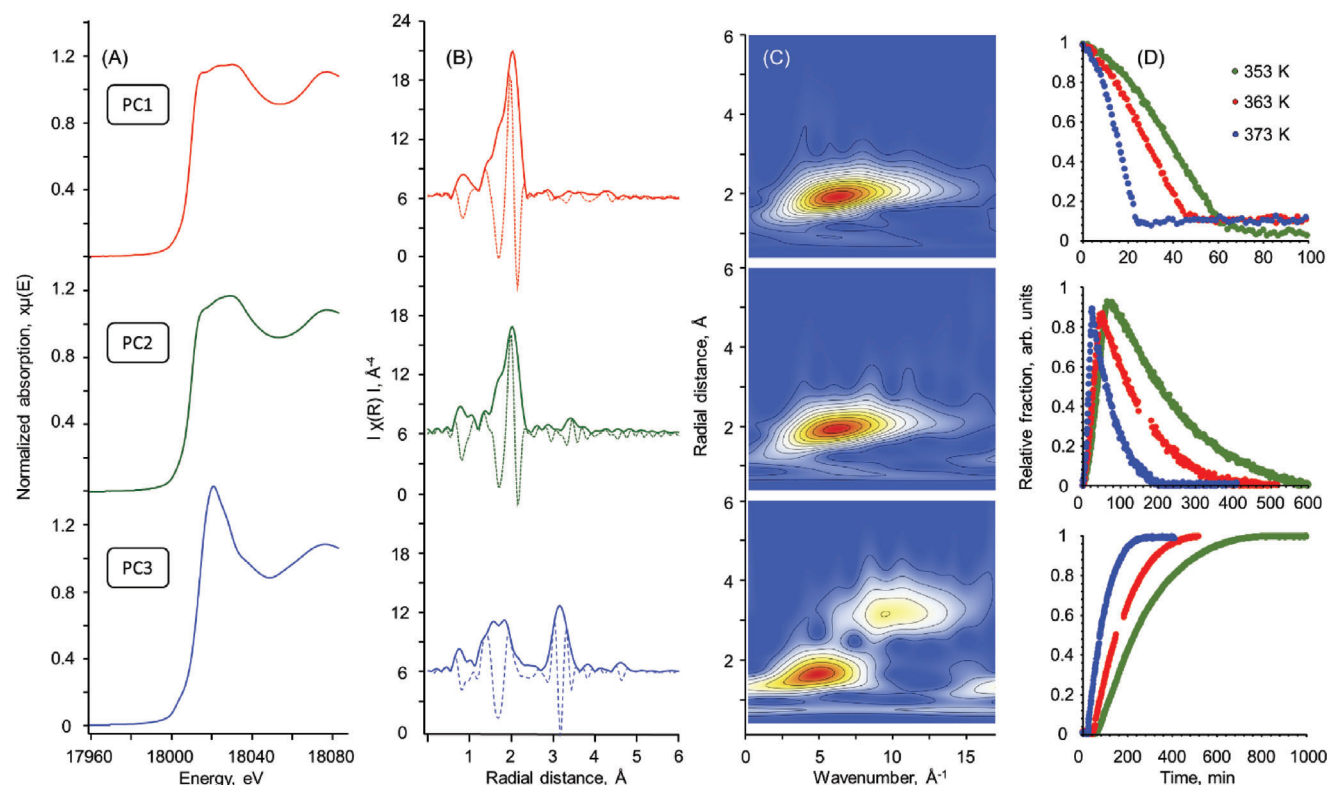
**ADVANCED
SCIENCE NEWS**

www.advancedsciencenews.com

NANO · MICRO

small

www.small-journal.com

Figure 3. Results of principal component analysis of the Zr K-edge time-resolved datasets in the temperature range of 353–373 K. A) PCA-resolved XANES spectra of three linearly independent components. B) Corresponding k^3-weighted FT EXAFS and C) WT EXAFS spectra, and D) evolution of the fraction of each principal component during the synthesis of UiO-66 at different temperatures. Different time scales for PC1-PC3 are used for the sake of clarity. Colored circles in (D) denote reaction temperature.

consumption from the solution. The duration of the plateau and the rate of depletion are governed by temperature. Apart from the concentration, the position of the terephthalate signal varies during the synthesis (Figure 4A). Plotting this signal position versus synthesis time shows that, initially, the chemical shift increases, passes through a maximum at about 167.66 ppm, and then decreases back to the original value of about 167.50 ppm (Figure 4E). This is explained in terms of the fast exchange between protonated and deprotonated terephthalate, coordinated to zirconium atoms. NMR spectroscopy, a relatively "slow" technique, probes the averaged state, and, therefore, the position of the peak varies depending on the relative fractions of the species involved in the chemical exchange. A shift to the lower field suggests an increase in the fraction of terephthalate species in the zirconium coordination sphere. Temporarily, the maxima of the terephthalate chemical shift coincide with the start of the consumption of terephthalate from the solution (Figure 4D,E; Figure S12, Supporting Information) at all the studied reaction temperatures. After comparing these data with the HRMS and XAS data sets, we conclude that the increase in the chemical shift of the terephthalate signals is associated with the formation of soluble zirconium chloroterephthalates. After reaching a certain exchange level, which we can not quantitatively estimate, the hydrolysis and formation of the UiO-66 solid nuclei begin, leading to a decrease in the intensity of the ^{13}C NMR signal. ^{1}H-^{13}C CP-MAS NMR spectra (Figure 4B) confirm this suggestion, showing the formation of solid terephthalate-containing species

giving a signal at 169.9 ppm after the induction period. It is worth noting that ^{1}H-^{13}C CP-MAS NMR spectra selectively detect rigid solidified particles, since in soluble and flexible species the polarization transfer is significantly hindered. These rigid species are likely represented by nuclei at short reaction times and crystalline MOF at the end of the reaction. The transient spectra contain both phases. The relative intensity of the signal plotted against the reaction time shows a gradual increase to a certain intensity, which is a function of the synthesis temperature. The decrease in the maximum CP-MAS NMR signal with increasing temperature is due to the less efficient polarization transfer, induced by the stronger dynamics, exchange, and relaxation. The weak interaction of dimethylformamine with zirconium and/or terephthalate hinders the polarization transfer from the abundant DMF protons, leading to a poor signal-to-noise ratio (Figure 4F).

Upon completion of the crystallization, the ^{13}C NMR spectrum without proton decoupling has several additional peaks (Figure 4G). The separate signal at 162.1 ppm is assigned to the free formate species, while a quartet centered at 35.1 ppm and possessing J_{CH}-splitting of 140 Hz is due to the dimethylammonium cation. Both are products of the hydrolysis of DMF. The ^{1}H-^{13}C CP-MAS NMR spectrum (Figure 4H) reveals the presence of a signal with an isotropic chemical shift of 169.9 ppm due to the terephthalate linker in the structure of UiO-66.[40] There is no signal due to formate in the spectrum, hence excluding its incorporation into the structure of the final MOF.
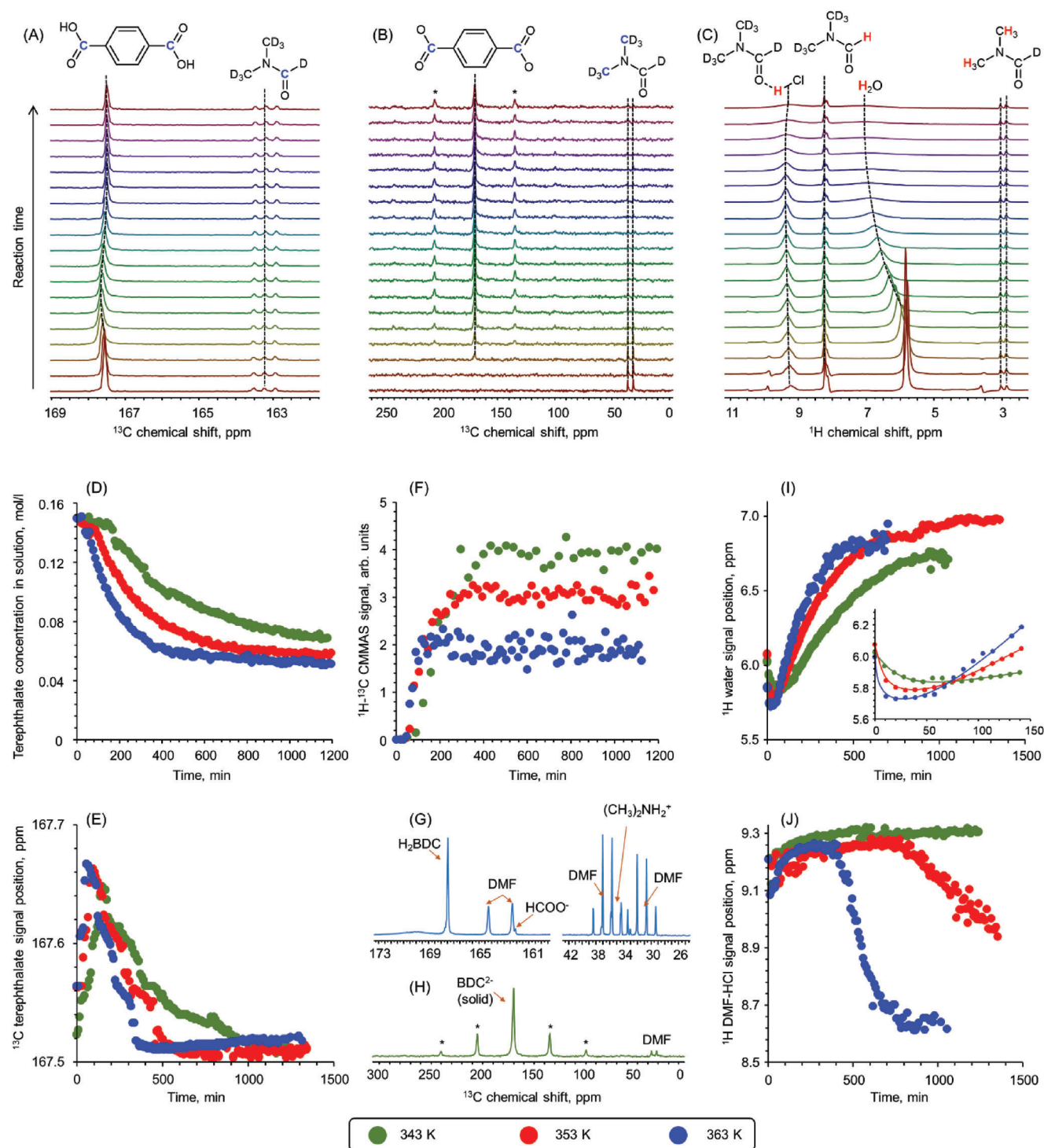
ADVANCED
SCIENCE NEWS

www.advancedsciencenews.com

NANO · MICRO
small
www.small-journal.com

Figure 4. Exemplary time-resolved A) ^{13}C NODEC, B) ^{1}H-^{13}C CP-MAS, and C) ^{1}H MAS NMR spectra acquired at 353 K, showing the gradual evolution of the terephthalate species in solution and in the solid phase as well as the fate of HCl and water during synthesis. D) Temporal evolution of the concentration and E) chemical shift of soluble terephthalate-containing species at different temperatures. F) Absolute intensity of the ^{1}H-^{13}C CP-MAS NMR signal due to the terephthalate in the course of the UiO-66 synthesis. G) ^{13}C NODEC and H) ^{1}H-^{13}C CP-MAS NMR spectra acquired at the end of the synthesis. I) Temporal evolution of the chemical shift of the signal due to water and J) DMF···HCl adduct during crystallization of UiO-66.
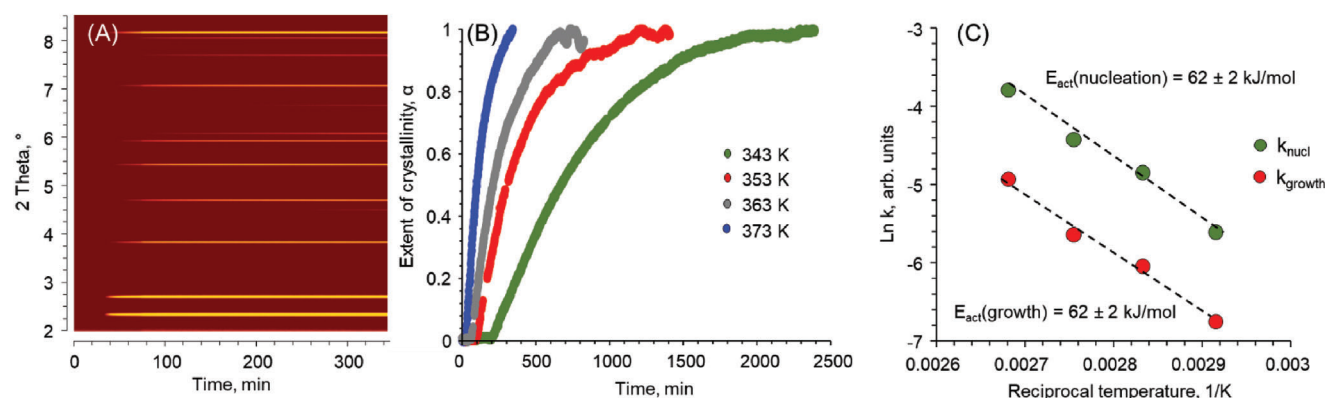
Figure 5. A) Time-resolved background-subtracted counterplots of XRD data recorded during the synthesis of UiO-66 at 373 K, B) extent of UiO-66 crystallinity obtained from the background-corrected XRD data, C) Arrhenius plots for k_g and k_n extracted from the corresponding fits using the Gualtieri model.

Zirconium atoms in the $[Zr_6(OH)_4O_4]$ node of UiO-66 are linked to bridging oxygen atoms and hydroxides, which originate from water present in a synthesis solution, that is, in the form of aqueous hydrochloric acid. ^{1}H NMR monitors the signals of H_2O as well as HCl (Figure 4C). Together with the signals due to the deuterated DMF (at 2.87, 3.04, and 8.2 ppm), there are two other signals with a varying chemical shift. The first signal between 5.5 and 7.0 ppm is assigned to water, while the second at about 9 ppm results from the DMF⋯HCl adduct.[36] The crystallization of UiO-66 leads to an irreversible change in the width of both signals, finally resulting in severe broadening, probably due to the inclusion of both compounds in the porous system of solid MOF. This does not enable an unambiguous integration of the peaks. Our discussion, therefore, is limited to the analysis of the positions of the peaks. Figure 4I displays the evolution of the chemical shift value of the water signal. It is evident that the reaction starts with some stabilization of the ^{1}H signal position during the induction period, which is followed by an exponential increase in the chemical shift to a stable value of ≈7.0 ppm. This is associated with an increase in the hydrochloric acid concentration due to the hydrolysis of zirconium chloride, accompanied by a decrease in the pH of the synthetic mixture. The position of the ^{1}H signal, due to the DMF⋯HCl adduct (Figure 4J), is stable at about 9.2 ppm, however, it starts to decrease rapidly after a reaction time, which is somewhat similar to the end of terephthalate consumption from the solution (Figure 4D) and stabilization of pH (Figure 4I). This signal also undergoes severe broadening (Figure 4C), and therefore we tentatively associate this behavior with the interaction of the DMF⋯HCl complex with the UiO-66 porous system.

In summary, the gradual exchange of zirconium chloride with terephthalic acid results in the formation of partially substituted soluble zirconium chloroterephthalates, which, in turn, undergo hydrolysis and form solid nuclei. HCl, another product of this exchange reaction, decreases the pH of the synthetic mixture and interacts with dimethylformamide, leading to the formation of a DMF⋯HCl adduct (interacting with UiO-66), which also undergoes hydrolysis, resulting in the dimethylammonium chloride and formate species in the supernatant solution.

2.4. In Situ X-Ray Diffraction

Figure 5A shows the evolution of the XRD pattern during the continuous heating of the synthetic mixture at 373 K.[28,29] After an induction period, the X-ray scattering data show the development of intense Bragg peaks at $2\Theta = 2.35°$ and $2.71°$, characteristic of UiO-66 ($Fm\bar{3}m$, cubic, $a = 20.755$ Å).[13,14] No other patterns belonging to phases, such as EHU-30, were found during the synthesis.[41] Notably, we did not observe any significant change in background shape and intensity during the synthesis, which makes the formation of amorphous clusters and particles, as was recently shown for ZIF-71, highly unlikely.[42] The background-corrected data were used to calculate the extent of crystallinity (Figure 5B). Between 343 and 373 K, the formation of UiO-66 starts with the induction period, followed by the progressive evolution of the crystalline phase. The increase in the reaction temperature strongly affects the crystallization kinetics, while the length of the induction period is affected to a lesser extent.[21] Comparing the crystallization profiles with the temporal behavior of the PC3 principal component extracted from XAS and corresponding to UiO-66 species (Figures 3D and 5B; Figure S13, Supporting Information) reveals a mismatch in the evolution of both curves. The signal due to the UiO-66 species in XAS appears earlier than that of the crystalline phase in XRD and it also reaches its maximum faster. We believe that X-ray absorption spectroscopy enables the detection of UiO-66 nuclei, which, spectroscopically, do not differ from the crystalline MOF phase. Certainly, zirconium atoms in UiO-66 nuclei possess identical to the crystals local environment, however, lacking long-range order, hence giving no XRD reflections. This is in line with ^{1}H-^{13}C CP-MAS NMR, demonstrating that there is no shift and/or split in the MOF signal during nucleation and growth (Figure 4B).

The quantitative analysis of the XRD kinetic profiles was performed according to the Gualtieri model (Equation (1)),[31] which enables temporal deconvolution of the nucleation and growth processes. According to the fitted values of the kinetic constants (Figure 5B), nucleation proceeds approximately ten times faster than growth in the studied temperature range. This indicates that growth is the rate-limiting step in the formation of the final UiO-66, this explains the average small size of about 200 nm
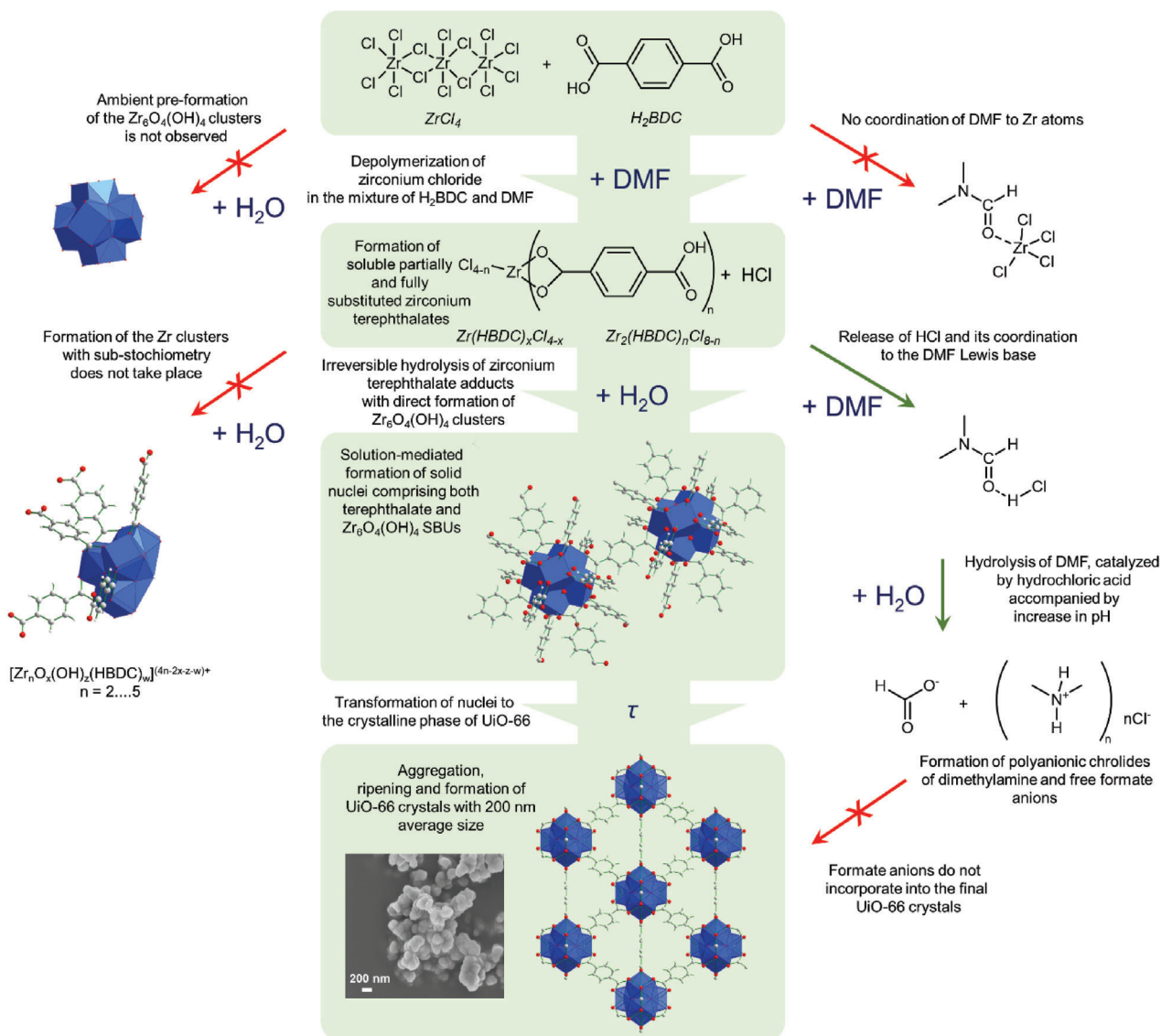
**ADVANCED
SCIENCE NEWS**

www.advancedsciencenews.com

NANO · MICRO

small

www.small-journal.com

Figure 6. Complete scheme of the molecular-level mechanism of UiO-66 nucleation and growth derived from time-resolved HRMS, Zr K-edge XAS, MAS NMR spectroscopy, and XRD data.

of the UiO-66 crystallites with a narrow size distribution (Figure S14, Supporting Information). The apparent activation energies, extracted from the Arrhenius plots (Figure 5C), correspond to 62 ± 2 kJ mol^{-1} for both nucleation and growth, in line with those previously reported for amino-functionalized UiO-66.[28] Assuming that X-ray absorption spectroscopy probes the initial stage of the nucleation phase, we have separately extracted the nucleation activation energy from the initial slopes of the kinetic curves due to PC3 XAS components at a different synthesis temperature (Figure S15a, Supporting Information). The obtained value, E_{nucl} = 54 ± 3 kJ mol^{-1} (Figure S15b, Supporting Information) is in line with the one extracted from the Gualtieri fitting, confirming our assumption.

$$\alpha = \frac{1}{1 + e^{-\frac{t-a}{b}}} \left(1 - e^{-\left(k_g t\right)^n} \right) \qquad (1)$$

where α—the extent of crystallinity, t—reaction time, k_g—rate constant for growth, a—reciprocal rate constant for nucleation, $k_n = 1/a$, b—variance of the nucleation probability distribution and n represent the dimensionality of crystal growth.

2.5. Discussion of UiO-66 Nucleation and Growth Mechanism

The synthesis of UiO-66 starts with the depolymerization of the solid zirconium chloride[43] in DMF to monomeric species and the autocatalytic formation of soluble zirconium chloroterephthalates, with a subsequent increase in the substitution degree and the number of terephthalate linkers in the zirconium coordination environment (**Figure 6**). In contrast to previous reports, the data in this work lacks evidence for the pre-formation of $[Zr_6(OH)_4O_4]$ nodes in the stock solution.[44] A by-product of

the exchange reaction is HCl, which accumulates in the solution, leading to a decrease in pH and the formation of a spectroscopically distinct DMF···HCl adduct. This adduct undergoes hydrolysis, catalyzed by HCl, leading to free formate species and various families of dimethylammonium chlorides, which can reversibly exchange with the metal cations, including Zr^{4+}.

In turn, after reaching a certain level of terephthalate exchange with zirconium chloride, the hydrolysis leading to the formation of the first nuclei starts (Figure 6). This process implies the rapid solution-mediated formation of the $[Zr_6(OH)_4O_4]$ nodes, with no stable sub-stoichiometric zirconium-oxo clusters being detected. The terephthalate linker becomes a part of the nuclei, while formate species formed by hydrolysis of DMF remain intact in the solution, in contrast to Al-containing MIL-53.[27] The nuclei are structurally identical to the secondary building units of UiO-66, however, they lack long-range order, which they gain during growth. Crystal growth represents the rate-limiting step in UiO-66 crystallization, with nucleation proceeding almost ten times faster, leading to many small crystals with a narrow size distribution of about 200 nm. The synthesis of the MOF ends with the stabilization of pH, the complete consumption of Zr precursors from the solution, and the absorption of residual water and HCl by the pore system of UiO-66. Dimethylammonium chloride and formate species are the main non-crystalline by-products remaining in the supernatant solution. Importantly, the cross-validation of the methods used in the present study (Figures S16–S19, Supporting Information) shows that the shape and size of reacting vessels as well as the spinning rate do not affect the crystallization kinetics and quality of products, and hence, conclusions drawn (see discussion in the Supporting Information).

3. Conclusions and Outlook

The crucial steps of the molecular-level mechanism of crystallization of one of the most important zirconium-containing MOFs are reported. The key role of zirconium chloroterephthalates, whose solution-mediated hydrolysis leads to rapid and irreversible UiO-66 nucleation, is demonstrated. Crystal growth is identified as the rate-limiting step, justifying the formation of the small crystals of UiO-66. *N, N*-dimethylformamide does not act as an inert solvent but rather undergoes gradual hydrolysis, thus forming non-crystalline by-products. The revealed complexity of the synthesis indicates that the simplification and generalization of the mechanisms in the crystallization of different MOFs must be avoided. In contrast, the case studies are required to rationalize and justify different synthetic protocols optimized for each particular MOF as well as to suggest novel, more sustainable routes. The combination of multiple advanced spectroscopic methods with kinetic measurements is essential to establish mechanisms of nucleation and growth. Our discovery advances the investigation of the synthesis of solids and will prompt scientific activity in this complex field, ultimately leading to the rational design of (novel) materials.

Supporting Information

Supporting Information is available from the Wiley Online Library or from the author.

Conflict Of Interest

The authors declare no conflict of interest.

Data Availability Statement

The data that support the findings of this study are available from the corresponding author upon reasonable request.

[1] H. Furukawa, K. E. Cordova, M. O'Keeffe, O. M. Yaghi, *Science* **2013**, *341*, 1230444.

[2] W. Lu, Z. Wei, Z.-Y. Gu, T.-F. Liu, J. Park, J. Park, J. Tian, M. Zhang, Q. Zhang, T. Gentle, M. Bosch, H.-C. Zhou, *Chem. Soc. Rev.* **2014**, *43*, 5561.

[3] G. Ferey, C. Mellot-Draznieks, C. Serre, F. Millange, J. Dutour, S. Surblé, I. A. Margiolaki, *Science* **2005**, *309*, 2040.

[4] K. Sumida, D. L. Rogow, J. A. Mason, T. M. McDonald, E. D. Bloch, Z. R. Herm, T.-H. Bae, J. R. Long, *Chem. Rev.* **2012**, *112*, 724.

[5] M. Ranocchiari, J. A. van Bokhoven, *Phys. Chem. Chem. Phys.* **2011**, *13*, 6388.

[6] J. Gascon, A. Corma, F. Kapteijn, F. X. Llabrés i Xamena, *ACS Catal.* **2014**, *4*, 361.

[7] J. Liu, L. Chen, H. Cui, J. Zhang, L. Zhang, C.-Y. Su, *Chem. Soc. Rev.* **2014**, *43*, 6011.

[8] J. Bachman, Z. Smith, T. Li, T. Xu, J. Long, *Nat. Mater.* **2016**, *15*, 845.

[9] D. Sheberla, J. Bachman, J. Elias, C. Sun, Y. Shao-Horn, M. Dinca, *Nat. Mater.* **2017**, *16*, 220.

[10] S. Yuan, L. Feng, K. Wang, J. Pang, M. Bosch, C. Lollar, Y. Sun, J. Qin, X. Yang, P. Zhang, Q. Wang, L. Zou, Y. Zhang, L. Zhang, Y. Fang, J. Li, H.-C. Zhou, *Adv. Mater.* **2018**, *30*, 1704303.

[11] Z. Chen, P. Li, R. Anderson, X. Wang, X. Zhang, L. Robison, L. Redfern, S. Moribe, T. Islamoglu, D. Gómez-Gualdrón, T. Yildirim, J. Fraser Stoddart, O. Farha, *Science* **2020**, *368*, 297.

[12] A. Bavykina, N. Kolobov, I. Khan, J. Bau, A. Ramirez, J. Gascon, *Chem. Rev.* **2020**, *120*, 8468.

[13] J. Cavka, S. Jakobsen, U. Olsbye, N. Guillou, C. Lamberti, S. Bordiga, K. Lillerud, *J. Am. Chem. Soc.* **2008**, *130*, 13850.

[14] L. Valenzano, B. Civalleri, S. Chavan, S. Bordiga, M. Nilsen, S. Jakobsen, K. Lillerud, C. Lamberti, *Chem. Mater.* **2011**, *23*, 1700.

ADVANCED
SCIENCE NEWS

www.advancedsciencenews.com

NANO · MICRO
small

www.small-journal.com

[15] J. Winarta, B. Shan, S. Mcintyre, L. Ye, C. Wang, J. Liu, B. Mu, *Cryst. Growth Des.* **2020**, *20*, 1347.

[16] R. Walton, F. Millange, *The Chemistry of Metal–Organic Frameworks: Synthesis, Characterization, and Applications* (Ed.: Stefan Kaskel), Wiley-VCH, Hoboken, NJ **2016**.

[17] N. Stock, S. Biswas, *Chem. Rev.* **2012**, *112*, 933.

[18] A. Schaate, P. Roy, A. Godt, J. Lippke, F. Waltz, M. Wiebcke, P. Behrens, *Chem. - Eur. J.* **2011**, *17*, 6643.

[19] Y. Zhao, Q. Zhang, Y. Li, R. Zhang, G. Lu, *ACS Appl. Mater. Interfaces* **2017**, *9*, 15079.

[20] F. Vermoortele, B. Bueken, G. Le Bars, B. Van de Voorde, M. Vandichel, K. Houthoofd, A. Vimont, M. Daturi, M. Waroquier, V. Van Speybroeck, C. Kirschhock, D. E. De Vos, *J. Am. Chem. Soc.* **2013**, *135*, 11465.

[21] F. Ragon, P. Horcajada, H. Chevreau, Y. Hwang, U. Lee, S. Miller, T. Devic, J. Chang, C. Serre, *Inorg. Chem.* **2014**, *53*, 2491.

[22] A. Ramanan, M. Whittingham, *Cryst. Growth Des.* **2006**, *6*, 2419.

[23] O. Shekhah, H. Wang, D. Zacher, R. Fischer, C. Woell, *Angew. Chem., Int. Ed.* **2009**, *48*, 5038.

[24] M. Rivera-Torrente, L. Mandemaker, M. Filez, G. Delen, B. Seoane, F. Meirer, B. Weckhuysen, *Chem. Soc. Rev.* **2020**, *49*, 6694.

[25] D. Cerasale, D. Ward, T. Easun, *Nat. Rev. Chem.* **2022**, *6*, 9.

[26] M. Van Vleet, T. Weng, X. Li, J. Schmidt, *Chem. Rev.* **2018**, *118*, 3681.

[27] D. Salionov, O. O. Semivrazhskaya, N. P. M. Casati, M. Ranocchiari, S. Bjelic, R. Verel, J. van Bokhoven, V. L. Sushkevich, *Nat. Commun.* **2022**, *13*, 3762.

[28] P. Schoenecker, G. Belancik, B. Grabicka, K. Walton, *AIChE J.* **2013**, *59*, 1255.

[29] M. Taddei, N. Casati, D. Steitz, K. Dümbgen, J. A. van Bokhoven, M. Ranocchiari, *CrystEngComm* **2017**, *19*, 3206.

[30] M. Goesten, M. de Lange, A. Olivos-Suarez, A. Bavykina, P. Serra-Crespo, C. Krywka, F. Bickelhaupt, F. Kapteijn, J. Gascon, *Nat. Commun.* **2022**, *7*, 11832.

[31] F. A Gualtieri, *Phys. Chem. Miner.* **2001**, *28*, 719.

[32] M. Avrami, *J. Chem. Phys.* **1939**, *7*, 1103.

[33] J. Hancock, J. Sharp, *J. Am. Ceram. Soc.* **1972**, *55*, 74.

[34] H. Xu, S. Sommer, N. Broge, J. Gao, B. Iversen, *Chem. - Eur. J.* **2019**, *25*, 2051.

[35] V. Guillerm, S. Gross, C. Serre, T. Devic, M. Bauer, G. Férey, *Chem. Commun.* **2010**, *46*, 767.

[36] M. Goesten, P. Magusin, E. Pidko, B. Mezari, E. Hensen, F., J. Kapteijn, J. Gascon, *Inorg. Chem.* **2014**, *53*, 882.

[37] G. Seeber, G. Cooper, G. Newton, M. Rosnes, D. Long, B. Kariuki, P. Koegerler, L. Cronin, *Chem. Sci.* **2010**, *1*, 62.

[38] A. Dighe, L. Huelsenbeck, R. Bhawnani, P. Verma, K. Stone, M. Singh, G. Giri, *JACS Au* **2022**, *2*, 453.

[39] M. Haouas, *Materials* **2018**, *11*, 1416.

[40] T. Bennett, T. Todorova, E. Baxter, D. Reid, C. Gervais, B. Bueken, B. van de Voorde, D. De Vos, D. Keen, C. Mellot-Draznieks, *Phys. Chem. Chem. Phys.* **2016**, *18*, 2192.

[41] S.-J. Lee, J. Mancuso, K. Le, C. Malliakas, Y.-S. Bae, C. Hendon, T. Islamoglu, Fahra, *ACS Mater. Lett.* **2020**, *2*, 499.

[42] S. Saha, S. Springer, M. Schweinefuß, D. Pontoni, M. Wiebcke, K. Huber, *Cryst. Growth Des.* **2016**, *16*, 2002.

[43] M. Kløve, R. Christensen, I. Nielsen, S. Sommer, M. Jørgensen, A.-C. Dippel, B. Iversen, *Chem. Sci.* **2022**, *13*, 12883.

[44] T. Lee, Y. Chang, H. Lee, *CrystEngComm* **2017**, *19*, 426.

2305771 (11 of 11)